Resonant domain wall depinning induced by oscillating spin-polarized currents in thin ferromagnetic strips

E. Martinez,[1,*] L. Lopez-Diaz,[2] O. Alejos,[3] and L. Torres[2]
[1]*Universidad de Burgos, Plaza Misael Banuelos s/n, E-09001 Burgos, Spain*
[2]*Universidad de Salamanca, Plaza de la Merced s/n, E-37008 Salamanca, Spain*
[3]*Universidad de Valladolid, Prado de la Magdalena, E-47071 Valladolid, Spain*
(Received 31 July 2007; revised manuscript received 24 January 2008; published 18 April 2008)

The interaction between ac spin-polarized electrical currents and a domain wall initially trapped on a notch in a thin Permalloy nanostrip is investigated by micromagnetic modeling as well as a one-dimensional model that considers the wall as a rigid object. A systematic study of the depinning transition from the notch is carried out in the frequency domain for several static magnetic fields and ac's, both at zero and at room temperature. Due to the resonant amplification of the domain wall oscillations, both the depinning current and the static magnetic field can be significantly reduced with respect to the dc case, and even at room temperature the probability of the domain wall depinning abruptly changes in a narrow frequency range. These observations suggest a low-operation and highly selective mode for further spintronic devices based on domain walls. On the other hand, our analysis is also used to estimate the effective value of the nonadiabatic parameter by direct comparison with recent experiments.

DOI: 10.1103/PhysRevB.77.144417 PACS number(s): 75.75.+a, 75.40.Mg, 75.40.Gb, 75.10.Hk

I. INTRODUCTION

Since the appearance of the pioneering works by Berger[1–3] and Slonczewski,[4,5] considerable progress has been made in understanding current-induced domain-wall (DW) dynamics in ferromagnetic strips.[6–14] The key mechanism is the spin torque from a spin-polarized current passing through a DW, where the spin of the itinerant conduction electrons couples to the local spatial gradient of the magnetization. Two forms of spin torque have been proposed so far: Adiabatic ($\xi=0$),[6,7] and nonadiabatic ($\xi>0$), where ξ represents the ratio between nonadiabatic and adiabatic torques.[6–10] The adiabatic case is expected to dominate for wide DWs, where the electron spin can adiabatically follow the slowly varying local spin direction as it goes through the DW. As the electron spin rotates, it exerts a torque on the DW normal to its plane of magnetization. If the spatial gradient in local magnetization across the DW is too large (thin DWs), a finite mistracking angle may develop between the electron spin and the local magnetization. This can result in spin-flip scattering of the electrons, and nonadiabatic pressure on the wall.[8] Without the action of an external magnetic field ($B_e=0$), the adiabatic torque due to static currents (dc) is not able to drive sustained DW motion except for very large currents (j_a). On the contrary, the nonadiabatic spin-transfer torque produces a force directly on the DW for static currents even in the absence of an external magnetic field. It has been shown that the adiabatic term is largely responsible for the initial DW velocity, while the nonadiabatic term controls its terminal velocity.[9]

Several experimental observations[15–19] indicate that both adiabatic and nonadiabatic effects should be present in some proportion for DWs with finite width. However, the exact value of the nonadiabatic parameter ξ is nowadays difficult to compute from first principles, and therefore, a study of the DW depinning from a notch as a function of the applied current j_a and the magnetic field B_e might help us to ascertain the magnitude of ξ by direct comparison between experiments and simulations.[14] Apart from pure fundamental interest, the analysis of the current-induced DW depinning is also of great technological relevance for designing novel domain-wall-based storage devices such as the Racetrack Memory.[20] The functionality of these spintronic devices requires the ability to control DW depinning, which can be achieved if sufficiently large static external magnetic fields and dc's j_a are applied with a duration in the nanosecond scale.[21–26] It has been observed that the DW depinning occurs only at zero or low magnetic fields if the static density current (dc) exceeds a threshold in the order of 10 A/μm^2.[14,24] Due to Joule heating,[15] such high current densities are impractical for spintronics applications,[24] and therefore it is crucial to find ways of reducing this threshold value.

The first experimental evidence of the low-current operation due to the resonant DW motion induced by oscillating currents was carried out by Saitoh *et al.*[27] They estimated the value of the effective DW mass by detecting its resonant motion in a semicircular Permalloy strip. Motivated by this observation, Tatara *et al.*[28] and then He *et al.*[29] studied the response of a pinned DW inside of a parabolic potential subjected to the action of ac in ferromagnetic films in the xy-plane with easy axis z perpendicular anisotropy. Using a deterministic one-dimensional description, they showed that the DW depinning occurs at a density current, which is lower than the dc case if the frequency is tuned close to the pinning frequency. Other experimental confirmation of this theoretical prediction was done by Thomas *et al.*[30] Using a train of current pulses with zero rise and fall times, they measured experimentally the probability of DW depinning from a notch in a straight strip at room temperature, and showed that the DW depinning can be efficiently achieved if the lengths and separations of the pulses are tuned to the characteristic pinning period. More recently, Bedau *et al.*[31] have evaluated the DW depinning from a notch in a Permalloy ring under static magnetic fields and sinusoidal ac's as a function of the

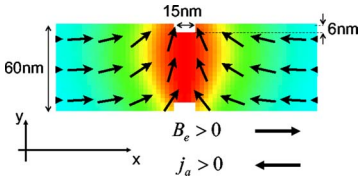

FIG. 1. (Color online) Schematic representation of the simulated geometry. The local magnetization configuration in absence of external field and current is depicted along with the direction and sign criteria for the external field $B_e = \mu_0 H_e$ and the applied current j_a.

frequency of the injected current. They observed a dip in the depinning field when the frequency of current matches the resonance frequency.

In the present paper, the DW dynamics induced by oscillating ac's, and also assisted by static magnetic fields, is systematically investigated in the frequency domain from a theoretical point of view. In Sec. II, DW dynamics induced by oscillating spin-polarized currents is analyzed by means of full micromagnetic modeling. Based on these micromagnetic results, the deterministic DW depinning is theoretically described in Sec. III by using a linearized one-dimensional model (1DM) which, in addition to the static forces, takes also into account the time-varying forces induced by the oscillating current as a function of its frequency. In order to get a more realistic description, the effect of thermal fluctuations has been also included in the analysis, and the probability of DW depinning is evaluated at room temperature in several cases. In Sec. IV, the experimental results by Bedau *et al.*[31] are fitted to the rigid approach, and the magnitude of the effective nonadiabatic parameter is deduced. A brief summary of the main conclusions is given in Sec. V.

II. MICROMAGNETIC SIMULATIONS

The system under study consists of a thin Permalloy strip with $L_y \times L_z = 60 \times 3$ nm^2 cross section where two notches (15 nm long and 6 nm wide) are symmetrically placed on both edges of the strip. A computational region of $L_x = 1.2$ μm in length, with the notch placed in the center, was discretized by means of a standard finite-difference scheme using cubic computational cells of $\Delta x = 3$ nm in side. Figure 1 depicts the equilibrium state of the DW at rest. The sign criteria for the positive fields and electrical density currents are also included in Fig. 1. Starting from this initial state, the dynamics of the local magnetization $\vec{M}(\vec{r})$ under the action of static magnetic fields $\vec{B}_e = B_e \vec{u}_x$ and spin-polarized electrical density currents $\vec{j}_{app}(t) = j_{app}(t)\vec{u}_x$, both of them spatially uniform and directed along the strip axis (x-axis), is described by the extended Landau–Lifshitz–Gilbert equation as derived from a quantum mechanical model by Zhang and Li,[9]

$$\frac{d\vec{M}}{dt} = -\gamma_0 \vec{M} \times \vec{H}_{eff} + \frac{\alpha}{M_s}\left(\vec{M} \times \frac{d\vec{M}}{dt}\right) + b_J(t)(\vec{u}_x \cdot \nabla)\vec{M} - \frac{c_J(t)}{M_s}\vec{M} \times (\vec{u}_x \cdot \nabla)\vec{M}, \quad (1)$$

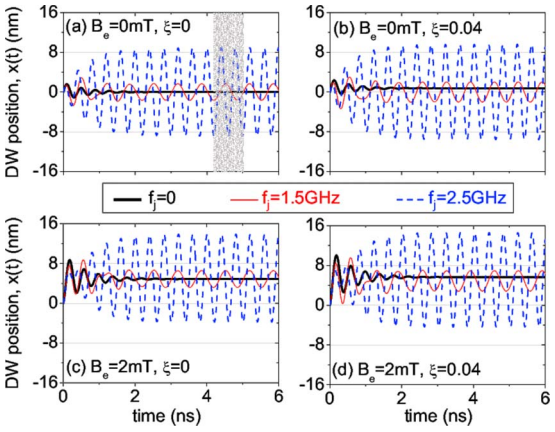

FIG. 2. (Color online) Micromagnetic results for the DW position $x(t)$ in pinned regime. A current in the form $j_{app}(t) = j_a \cos(2\pi f_j t)$ is applied with fixed amplitude $j_a = 1.25$ A/μm^2 and three different frequencies: $f_j = 0$ (dc case, black-thick solid lines), $f_j = 1.5$ GHz (red-thin solid lines), and $f_j = 2.5$ GHz (blue dash lines). The DW dynamics at zero field ($B_e = 0$) is depicted in top graphs (a) and (b) for the perfect adiabatic limit ($\xi = 0$) and finite nonadiabatic corrections ($\xi = 0.04$), respectively. The corresponding DW oscillations assisted by a static field of $B_e = 2$ mT are represented in bottom graphs (c) and (d).

where γ_0 is the gyromagnetic ratio, α is the Gilbert damping parameter, M_s is the saturation magnetization, and $\vec{H}_{eff}$ is the effective field, which includes exchange, self-magnetostatic and external field contributions.[13] The last two terms on the right side of Eq. (1) represent the adiabatic and the nonadiabatic spin-transfer torques, respectively.[9] The coefficients $b_J(t)$ and $c_J(t)$ are given by $b_J(t) = j_{app}(t)\frac{\mu_B P}{eM_s}$ and $c_J(t) = \xi b_J(t)$, where μ_B is the Bohr magneton, P the spin polarization factor of the current, and $e < 0$ the electron's electric charge. The coefficient ξ is a dimensionless constant describing the degree of nonadiabaticity between the spin of conduction electrons and the local magnetization.[8] Typical Permalloy parameters were considered: saturation magnetization $M_s = 860$ kA/m, exchange constant $A = 13$ pJ/m, damping $\alpha = 0.02$, and polarization factor $P = 0.4$. All numerical details of our micromagnetic code can be found elsewhere.[13]

In the present work, time-varying electrical density currents in the form $j_{app}(t) = j_a \cos(2\pi f_j t)$ are applied along with static magnetic fields $B_e \neq f(t)$. Typical micromagnetic results of the pinned regime are shown in Fig. 2. The amplitude of applied density current is $j_a = 1.25$ A/μm^2, and three different frequencies are considered: $f_j = 0$ (dc case, black-thick lines), $f_j = 1.5$ GHz (red-thin lines), and $f_j = 2.5$ GHz (blue-dash lines). The DW position is micromagnetically computed as $x = \frac{L_x}{2}\langle m_x \rangle$, where $\langle m_x \rangle$ represents the x-component of the averaged magnetization over the computational region. Top graphs in Figs. 2(a) and 2(b) depict the temporal evolution of the DW position $x(t)$ excited by the mentioned currents in absence of external field $B_e = 0$ for both perfect adiabatic ($\xi = 0$) and nonadiabatic ($\xi = 0.04$) cases, respectively. On the other hand, bottom graphs of Figs. 2(c) and 2(d) show the current-induced DW dynamics assisted by a static magnetic field of $B_e = 2$ mT for $\xi = 0$ and

ξ=0.04, respectively. For dc's (f_j=0) (see black-thick lines in Fig. 2), the DW position $x(t)$ develops damped oscillations, which attenuate in time as due to the damping, and the wall finally reaches a new terminal equilibrium position ($x(\infty)$). The external force exerted by both the dc and the static field, is balanced by the restoring force derived from the pinning potential of the notch. At zero field, the DW position $x(t)$ returns to the initial state in the perfect adiabatic limit [ξ=0, Fig. 2(a)], whereas a positive displacement is observed if nonadiabatic corrections are considered [$\xi>0$, Fig. 2(b)]. Only in the presence of a positive magnetic field [Fig. 2(c)] the terminal DW position is displaced to the right in the perfect adiabatic case. The characteristic frequency $f_{N,\mu M}$ of the damped oscillations was computed from the Fourier transform of the $x(t)$,[13] and a sharp peak is observed at $f_{N,\mu M} \approx 2.5 \pm 0.1$ GHz independently of ξ.

A more interesting DW dynamics can be excited by ac's ($f_j>0$). As it is shown in Fig. 2, after a short transient time, the DW position $x(t)$ reaches stationary regime and oscillates with constant amplitude at the same frequency (f_j) as the ac $j_{app}(t)$. The oscillations of $x(t)$ are symmetrical with respect to the center of the notch at zero field [see Figs. 2(a) and 2(b)]. An analogous behavior is observed in the presence of a static field B_e=2 mT [see Figs. 2(c) and 2(d)] but now the center around which the DW oscillations take place is displaced to the right as due to the external field driven force. For finite nonadiabatic corrections (ξ=0.04), the amplitude of the stationary DW oscillations is slightly increased with respect to the perfect adiabatic case (ξ=0), but most importantly, in both cases the amplitude of the DW oscillations is resonantly amplified when the frequency f_j of the current coincides with the natural frequency of the pinning potential of the notch $f_{N,\mu M}$.[14] This is an important observation for further technological applications, because it indicates that the DW depinning can be achieved by means of much more smaller currents than in the dc case if the frequency of the ac becomes close to the characteristic frequency of the system.

For a more detailed description of the micromagnetic results, we focus our attention on the zero field (B_e=0) and perfect adiabatic (ξ=0) resonant DW oscillations driven by an ac of j_a=1.25 A/μm^2 and f_j=2.5 GHz. Two complete periods (T=0.4 ns) of the stationary regime are depicted in the left panel of Fig. 3 corresponding to the shaded interval in Fig. 2(a). The instantaneous applied current is represented in Fig. 3(a). The temporal evolution of the DW position $x(t)$ and velocity $v(t)=\frac{\partial x}{\partial t}$ are depicted in Fig. 3(b). In order to quantify the current-induced DW distortion, the temporal evolution of the normalized DW width[33] to its static value $\Delta(t)/\Delta_0$ is also monitored in Fig. 3(c). Snapshot images of the spatial distribution of the magnetization $m_y(\vec{r})=M_y(x,y)/M_s$ are collected in right panels at five different instants: (d) t=4.3 ns, (e) t=4.4 ns, (f) t=4.5 ns, (g) t=4.6 ns, and (h) t=4.7 ns from top to bottom, respectively. In this stationary regime, the DW position $x(t)$ oscillates at the same frequency and in phase with the applied current $j_{app}(t)$ [see Figs. 3(a) and 3(b)]. As it is shown in Fig. 3(b), the DW velocity $v(t)$ also oscillates with the same current frequency f_j but it is advanced a quarter of a period ($T/4$=0.1 ns) with respect to both $j_{app}(t)$ and $x(t)$. That is, the DW position $x(t)$ and the applied current $j_{app}(t)$ are maximum or minimum when the DW velocity $v(t)$ is null, and vice versa. On the other hand, the DW width $\Delta(t)$ [Fig. 3(c)] oscillates twice faster than the DW position $x(t)$.

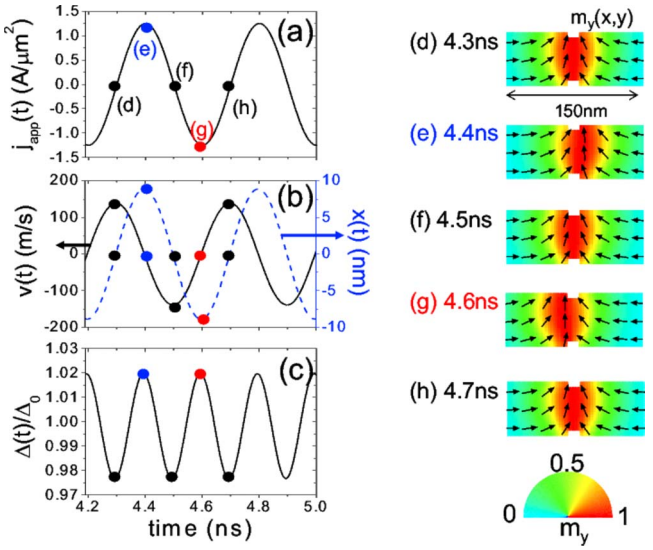

FIG. 3. (Color online) Micromagnetic details of the stationary regime reached for B_e=0, j_a=1.25 A/μm^2, ξ=0, and f_j=2.5 GHz corresponding to the shaded interval in Fig. 2(a).

As depicted in Figs. 3(d)–3(h), the DW width is a minimum when the wall is at the center (x=0), and it reaches a maximum in the extrema of the DW oscillations $x=\pm A_{S,\mu M}$, where $A_{S,\mu M}$ represents the micromagnetically computed amplitude of the current-induced DW oscillations in the stationary regime. It is to be noted that the largest deviation of the DW width $\Delta(t)$ from its static value Δ_0 remains smaller than the 3% even in the resonance. Therefore, these micromagnetic simulations indicate that the DW behaves, in good approximation, like a damped harmonic oscillator forced by an ac.

III. LINEARIZED ONE-DIMENSIONAL MODEL

A. Deterministic case, T=0 K

Our main interest here consists in calculating the threshold depinning amplitude j_a of the ac applied current $j_{app}=j_a \cos(2\pi f_j t)$, which produces DW depinning as a function of the frequency f_j in the presence of static field $B_e=\mu_0 H_e$. Due to the large number of amplitudes j_a, frequencies f_j, and fields B_e that have to be evaluated, the analysis requires a lot of computational effort if it is carried out by means of full micromagnetic simulations. The problem becomes inaccessible if, as it is desirable for getting more realistic results, the effect of thermal fluctuations needs to be taken into account. Due to these computational limitations, and in order to get a further understanding on how the DW depinning from the notch depends on (B_e,j_a,f_j), a rigid one-dimensional description will be adopted in the rest of the discussion, which allows us to systematically analyze the influence of thermal effects in the DW depinning process with manageable computational effort.

The 1DM was originally introduced to describe the deterministic field-driven motion of DWs,[32] and it has been re-

cently extended to include spin torque[7–10,28,29] and thermal effects.[13,14,34] The linearized version of the 1DM assumes that (i) the DW width remains constant independently of the field and the current (Δ_0=21.14 nm),[33] and (ii) the tilt angle between the magnetization and the easy plane (xy-plane) is very small.[12] Both of them are fulfilled in our case. Therefore, in the absence of thermal fluctuations, DW dynamics can be described by the following deterministic equation:

$$(1+\alpha^2)m_w\frac{d^2x}{dt^2} = F_p(x) + F_f + F_{e,s} + F_{e,d}, \tag{2}$$

where $m_w = \frac{2(\mu_0 L_y L_z)}{\gamma_0^2(N_z - N_y)\Delta_0}$ is the effective DW mass being N_y and N_z the transverse demagnetizing factors.[35] A value of $m_w = 5.25\times10^{-25}$ kg is obtained for the DW at rest. The terms on the right hand side of Eq. (2) are the different contributions to the total force acting on the DW. The first one, $F_p(x)$, is the spatially dependent restoring force derived from the pinning parabolic potential $V_{pin}(x)$ associated with the notch. Based on the micromagnetic characterization done in Ref. 14, the pinning force is given by

$$F_p(x) = -\frac{\partial V_{pin}(x)}{\partial x} = \begin{cases} -K_N x & (|x| \le L_N) \\ 0 & (|x| > L_N), \end{cases} \tag{3}$$

where K_N is the elastic constant of the notch, which was computed from the slope of the linear behavior of the elongation as a function of the field-driven force, yielding a value of $K_N = 1.3\times10^{-4}$ N/m. The natural frequency of the one-dimensional free harmonic oscillator is therefore given by $f_N = \frac{1}{2\pi}\sqrt{\frac{K_N}{m_w}} = 2.5$ GHz, in good agreement with the micromagnetic simulations. The length of the pinning potential, L_N=16 nm, was deduced by fitting the depinning threshold field obtained micromagnetically.[14]

The second one, F_f, is the friction force, which is proportional to the DW velocity $v = \frac{dx}{dt}$ and the damping parameter α,

$$F_f = -\left[\alpha m_w \omega_d \left(1 + \frac{\omega_N^2}{\omega_d^2}\right)\right]\frac{dx(t)}{dt} = -b\frac{dx(t)}{dt}, \tag{4}$$

where $\omega_d = \gamma_0 M_s(N_z - N_y)$ is the angular frequency of magnetization oscillations around the demagnetizing field inside the wall, and $\omega_N = 2\pi f_N$.

The last two terms on the right hand side of Eq. (2) represent the static ($F_{e,s}$) and dynamical ($F_{e,d}$) contributions to the external driving force. The static driving force $F_{e,s}$ has two contributions: one related to the external magnetic field $H_e = B_e/\mu_0$, and the other relative to the applied current j_a,

$$F_{e,s} = F_{H,s} + F_{j,s} = m_w\omega_d(\gamma_0\Delta_0 H_e - c_J). \tag{5}$$

The time-varying contribution $F_{e,d}$ to the external driving force has also two contributions associated with the time variation of the field and the current, respectively, and it is given by

$$F_{e,d} = F_{H,d} + F_{j,d} = m_w\left[\alpha\gamma_0\Delta_0\frac{\partial H_e(t)}{\partial t} - (1+\alpha\xi)\frac{\partial b_J(t)}{\partial t}\right]. \tag{6}$$

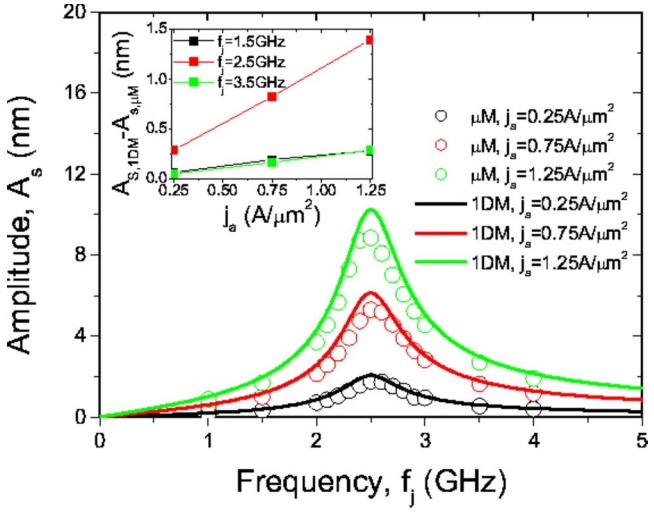

FIG. 4. (Color online) Amplitude of stationary DW oscillations as a function of the frequency of the oscillating current (f_j) for B_e =0 mT, and ξ=0. Micromagnetic results ($A_{S,\mu M}$, represented by dots) are compared with 1DM predictions ($A_{S,1DM}$, represented by lines), which are given by Eq. (A6) for three different values of j_a. The inset depicts the stationary amplitude differences between 1DM and μM values for three different frequencies as a function of j_a.

In the present analysis, we restrict our attention to the case of static applied fields, and therefore, $\frac{\partial H_e}{\partial t}$=0 is considered in Eq. (6).

The deterministic analytical solution for Eq. (2) describing the temporal evolution of the DW position $x(t)$ inside of an infinite harmonic potential well is presented in the Appendix. It is easy to verify that the analytical solution [Eq. (A1) with Eqs. (A2) and (A4)] leads to the same features of the micromagnetic trajectories for the DW oscillations depicted in Fig. 2. In order to compare the 1DM predictions with former micromagnetic observations (μM) of the previous section, the amplitude of the DW oscillations as a function of the frequency f_j is depicted in Fig. 4 for three different amplitudes j_a of the ac in the pinned stationary regime. Both models predict the same stationary behavior, but the amplitude is slightly overestimated by the 1DM with respect to the micromagnetic results (μM) for frequencies close to the resonance. The inset of Fig. 4 shows the difference $A_{S,1DM} - A_{S,\mu M}$ for three different frequencies. As it is observed, the discrepancies between the 1DM and the micromagnetic (μM) simulations increase linearly with the amplitude j_a of the applied current, and they are more significant for frequencies close to the resonance. These discrepancies are due to the fact that the 1DM does not take into account the change in the DW width, which increases with j_a. Nevertheless, even in the resonance the deviations of the DW width with respect to its static value are very small [<3%, see Fig. 3(c)], and therefore, the 1DM appears to describe well accurately the essential resonant behavior of the DW oscillations around the notch.

Once the pinned oscillations have been described, we focus on the analysis of the DW depinning predicted by the 1DM. The general solution (A1) with Eqs. (A2) and (A4) describes the temporal evolution of the DW position inside

an infinite harmonic potential well from a linearized one-dimensional point of view. Taking into account the finite length L_N of the parabolic potential induced by the notch, the critical depinning curves can be computed by evaluating the general solution (A1) with Eqs. (A2) and (A4), and the DW depinning takes place at a given time if $x(t) \geq L_N$.

We first compute the depinning field as a function of (ξ, f_j, j_a). Due to the characteristic time describing the transient regime $t_T = 2m_w/b$ is small ($t_T = 0.68$ ns), a first approach can be done by neglecting the transient regime ($t \gg T$). In such a case, the condition for DW depinning is given by the stationary part ($x_S(t)$) of the general solution [see Eq. (A4)]. Taking the maximum value of the stationary DW position $|x_S(t)|_{max}$ equal to the length of the pinning potential L_N, $|x_S(t)|_{max} = x_{eq,H} + A_S = L_N$, we obtain the following expression for the stationary depinning field $B_{dep,S}(\xi, f_j, j_a) = \mu_0 H_{dep,S}$ as function of the nonadiabatic parameter ξ, and both the amplitude j_a and the frequency $\omega_j = 2\pi f_j$ of the injected current,

$$B_{dep,S}(\xi, f_j, j_a) = B_{dep}^{j_a=0} + \mu_0 \beta(\xi, f_j) j_a, \tag{7}$$

where $B_{dep}^{j_a=0}$ represents the depinning field in the absence of current,

$$B_{dep}^{j_a=0} = \frac{K_N L_N}{(L_y L_z) 2M_s}, \tag{8}$$

and the dependence of $B_{dep,S}(\xi, f_j, j_a)$ on both $\omega_j = 2\pi f_j$ and ξ is enclosed in the function $\beta(\xi, f_j)$,

$$\beta(\xi, f_j) = \frac{1}{\gamma_0 \Delta_0} \frac{\mu_B P}{e M_s} \omega_N^2 \sqrt{\frac{\xi^2 + (1+\alpha\xi)^2 \frac{\omega_j^2}{\omega_d^2}}{(\omega_N^2 - \omega_j^2)^2 + \left(\frac{b}{m_w}\right)^2 \omega_j^2}}. \tag{9}$$

The stationary critical depinning field given by Eq. (7) represents the minimum field required to depin the DW from the notch for given values of ξ, f_j, and j_a. The stationary depinning fields $B_{dep,S}(\xi, f_j, j_a) = \mu_0 H_{dep,S}$ for DW depinning are plotted by solid lines in Fig. 5(a) as a function of the frequency f_j of the injected current for a constant density current of $j_a = 1$ A/μm^2, and several values of the nonadiabatic parameter ξ. For combinations of B_e and f_j below (above) each curve of Fig. 5(a), the DW remains pinned in (is depinned from) the notch. The critical curve separates the pinned (denoted as "P") from the depinned ("D") phase. The stationary depinning field $B_{dep,S}(\xi, f_j, j_a)$ monotonously decreases with increasing ξ, and it depicts a dip at the resonance frequency ($f_j = f_N$). The same analysis was also carried out by evaluating the general solution (A1), which not only takes into account the stationary regime (A4), but it also includes the transient dynamics given by Eq. (A2). The obtained depinning fields $B_{dep}(\xi, f_j, j_a)$ are depicted by dots in Fig. 5(a).

As in the stationary case, the depinning field $B_{dep}(\xi, f_j, j_a)$ depicts a pronounced dip at the resonance frequency, and it decreases with increasing ξ in the whole frequency range. The inset of Fig. 5(a) represents the difference $B_{dep,S} - B_{dep}$ as

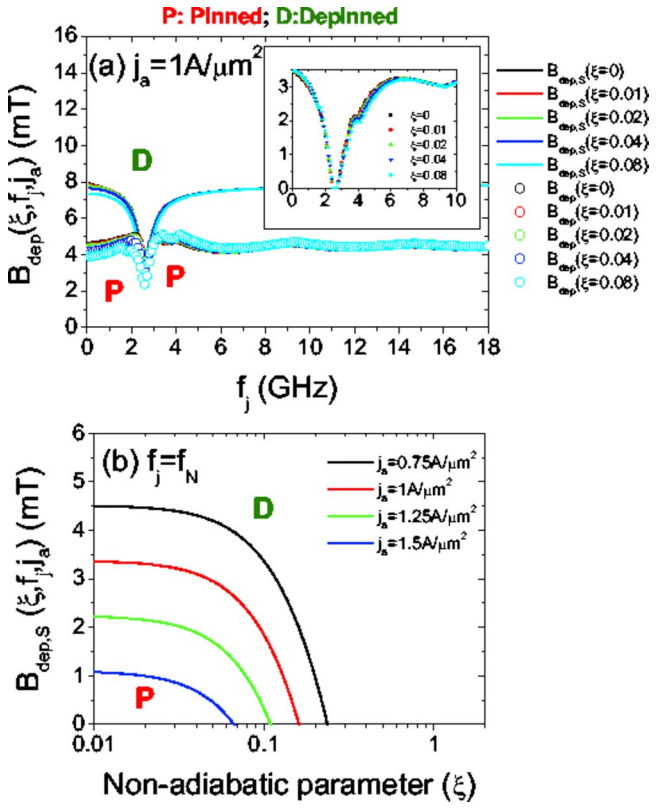

FIG. 5. (Color online) (a) Critical depinning field $B_{dep}(\xi, f_j, j_a) = \mu_0 H_{dep}$ as a function of the frequency f_j for a constant amplitude of the density current $j_a = 1$ A/μm^2, and several values of the nonadiabatic parameter ξ predicted by the 1DM. Solid lines represent the stationary depinning field $B_{dep,S}(\xi, f_j, j_a)$ computed from Eq. (7), whereas dots correspond to the depinning field including both the transient and stationary regimes $B_{dep,}(\xi, f_j, j_a)$. The inset shows the difference $B_{dep,S} - B_{dep}$ as a function of the frequency f_j. (b) Depinning field as a function of the nonadiabatic parameter ξ at resonance ($f_j = f_N$) for several values of the current j_a. The critical curves separate the pinned (denoted as P) from the depinned (D) phase.

function of f_j for several values of ξ. In the dc case ($f_j = 0$), the stationary depinning field ($B_{dep,S}$) prediction overestimates the depinning field with respect to the general solution (B_{dep}) because the stationary criterion does not take into account the initial velocity $v(0) = -\frac{b_J(0)}{1+\alpha^2}$ due to the adiabatic term. On the other hand, the stationary depinning field ($B_{dep,S}$) becomes equal to the general case (B_{dep}) at the resonance ($f_j = f_N$), and both of them depict the same dependence on the nonadiabatic parameter ξ, which is given by Eq. (7). Figure 5(b) illustrates the dependence of $B_{dep,S}(\xi, f_j = f_N, j_a)$ on the nonadiabatic parameter ξ for several values of the applied density current. For $j_a = 0.75$A/μm^2, $B_{dep,S} = B_{dep} = 4.5$ mT in the perfect adiabatic limit, and it slightly decreases for $0 \leq \xi \leq \alpha$. $B_{dep,S}$ starts to decrease stronger when ξ approaches 5α, and it becomes zero for $\xi \approx 12\alpha$. As j_a increases, the critical curve moves toward smaller values of both $B_{dep,S}$ and ξ.

We now focus on describing the depinning current as a function of (ξ, f_j, B_e). From the stationary depinning criterion ($|x_S(t)|_{max} = L_N$), the stationary depinning current

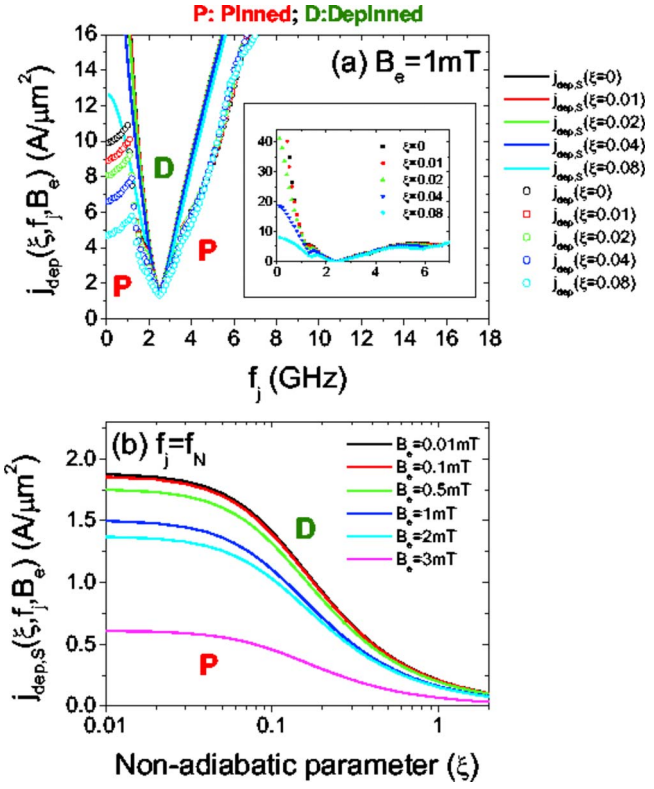

FIG. 6. (Color online) (a) Critical depinning current $j_{dep}(\xi,f_j,B_e)$ as a function of the frequency f_j under constant field $B_e=1$ mT, and several values of the nonadiabatic parameter ξ predicted by the 1DM. Solid lines indicate the stationary depinning current $j_{dep,S}(\xi,f_j,B_e)$ computed from Eq. (10), whereas dots correspond to the depinning current $j_{dep}(\xi,f_j,B_e)$ including both the transient and stationary regimes. The inset show the difference $j_{dep,S}-j_{dep}$ as a function of f_j. (b) Depinning current as a function of the nonadiabatic parameter ξ at resonance ($f_j=f_N$). The critical curves separate the pinned (denoted as P) from the depinned (D) phase.

$j_{dep,S}(\xi,f_j,B_e)$ can be expressed in terms of the depinning field at zero current $B_{dep}^{j_a=0}$ as

$$j_{dep,S}(\xi,f_j,B_e)=\frac{1}{\mu_0\beta(\xi,f_j)}(B_e-B_{dep}^{j_a=0}). \tag{10}$$

The stationary depinning current $j_{dep,S}(\xi,f_j,j_a)$ required to depin the DW from the notch are plotted by solid lines in Fig. 6(a) as a function of the frequency f_j of the injected current for a constant field of $B_e=1$ mT, and several values of the nonadiabatic parameter $0\leq\xi\leq4\alpha$. For combinations of j_a and f_j below (above) each curve of Fig. 6(a), the DW remains pinned in (is depinned from) the notch. The stationary depinning current $j_{dep,S}(\xi,f_j,B_e)$ decreases with increasing ξ, and it depicts a dip at the resonance frequency ($f_j=f_N$). The dots in Fig. 6(a) show the frequency dependence of critical depinning current j_{dep} when the transient dynamics is taken into account. As in the stationary case, the depinning current $j_{dep}(\xi,f_j,B_e)$ decreases with increasing ξ, and it also depicts a dip at resonance. As it is observed in the inset of Fig. 6(a), which depicts $j_{dep,S}-j_{dep}$ versus f_j, the stationary criterion significantly overestimates the depinning current

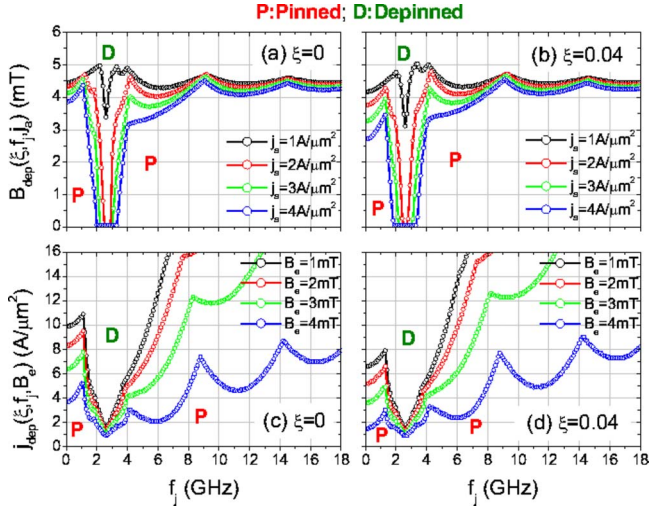

FIG. 7. (Color online) Critical depinning curves as computed from the 1DM at zero temperature. In the top panels, the critical depinning fields $B_{dep}(\xi,f_j,j_a)$ as a function of the frequency f_j for several values of the applied current j_a are depicted in (a) and (b) for $\xi=0$ and $\xi=0.04$, respectively. In the bottom ones, the critical depinning currents $j_{dep}(\xi,f_j,B_e)$ as a function of the frequency f_j are depicted in (d) and (d) for $\xi=0$ and $\xi=0.04$, respectively, for several values of the external field B_e. Each critical curve represents the minimum field (top graphs) or current (bottom graphs) needed to depin the DW from the notch as a function of the frequency, and they separate the pinned (denoted as P) from the depinned (D) phase.

with respect to the full solution for $f_j=0$. However, both $j_{dep,S}$ and j_{dep} are equal at resonance. Figure 6(b) shows the dependence of $j_{dep,S}$ on ξ at the resonance for several values of the static field B_e.

The results of former Fig. 5(a) (Fig. 6(a)) describe the frequency dependence of B_{dep} (j_{dep}) on ξ under constant current $j_a=1$ A/μm^2 (under constant field $B_e=1$ mT). The top graphs of Fig. 7 show the frequency dependence of B_{dep} for four values of the current j_a, and for both (a) $\xi=0$ and (b) $\xi=0.04$, respectively. These results were obtained from the general solution given by Eq. (A1) with Eqs. (A2) and (A4), as described in the Appendix. For combinations of B_e and f_j below (above) each curve of Fig. 7, the DW remains pinned in (is depinned from) the notch. The critical depinning field $B_{dep}(\xi,f_j,j_a)$ decreases as the amplitude of the ac is increased in the whole frequency range. DW depinning can be achieved with a minimum field of 3.4 mT ($\xi=0$) at the resonance frequency for $j_a=1$ A/μm^2. As it is shown, the minimum depinning field slightly decreases to 3.1 mT if ξ increases to 0.04. If $j_a=2$ A/μm^2, the minimum depinning field almost vanishes in a narrow frequency range around the resonance (2.4 GHz$\leq f_j\leq$2.7 GHz, for $\xi=0$). This depinning range of frequencies becomes wider if j_a is further augmented, as it is clear from Figs. 7(a) and 7(b) for $j_a=3$ A/μm^2 and $j_a=4$ A/μm^2.

The critical depinning current $j_{dep}(\xi,f_j,B_e)$ as a function of the frequency f_j is shown in the bottom graphs of Fig. 7 for $\xi=0$ (c) and $\xi=0.04$ (d), respectively. Four different values of the external field B_e are depicted. As it was expected, the depinning threshold current decreases as the static field is

increased in the whole frequency range. Due to the amplification of the DW oscillations, the threshold values of both B_{dep} [Figs. 7(a) and 7(b)] and j_{dep} [Figs. 7(c) and 7(d)] are significantly reduced with respect to the dc case when the frequency of the ac f_j matches the resonance frequency f_N. For instance, if the applied field is fixed to $B_e=1$ mT with $\xi=0$, the minimum depinning density current is 1.5 A/μm^2 in resonance, which represents a reduction by a factor of more than 5 as compared to the dc case [see Fig. 7(c)]. These deterministic phase diagrams suggest different experimental procedures to manipulate pinned DWs by using the concept of the resonant amplification with low currents. For example, a fixed amplitude of $j_a=2$ A/μm^2 is enough to promote the DW depinning just if the frequency of the current is properly chosen [see Figs. 7(a) and 7(b)], and the velocity of the subsequent DW free propagation can be controlled by different static external fields.

B. Thermal effects, $T=300$ K

The results of the previous subsection were computed at zero temperature. They provide a reasonably accurate description of measurements made at low temperatures. However, most of the experiments are done at room temperature $T=300$ K where thermal effects are important. In order to get more realistic insight of the depinning process, thermal fluctuations are included in the 1DM formalism through the addition of a random thermal force $F_t(t)$ on the right side of Eq. (2). $F_t(t)$ is uncorrelated in time and obeys a purely Gaussian distribution with zero average value and variance $2D_{1D}$ (Ref. 13):

$$\langle F_t(t)\rangle = 0, \tag{11}$$

$$\langle F_t(t)F_t(t')\rangle = 2D_{1D}\delta(t-t'). \tag{12}$$

The factor D_{1D} represents the strength of the thermal force, which was derived from the fluctuation-dissipation theorem,[13]

$$D_{1D} = \mu_0 L_y L_z M_s \frac{2\alpha K_B T}{\gamma_0 \Delta_0}. \tag{13}$$

Finite temperatures introduce fluctuations in the system, and therefore the deterministic behavior described in the former subsection becomes stochastic. With the aim of describing how thermal fluctuations at room temperature ($T=300$ K) modify the deterministic DW depinning, stochastic equation (2), which includes $F_t(t)$ on the right hand side, is numerically solved by means of a fourth-order Runge–Kutta scheme imposing an initial velocity of $v(0)=-\frac{b_J(0)}{(1+\alpha^2)}$.[8,13] The temporal evolution of the DW is evaluated during a fixed temporal window of $t_w=100$ ns, and the probability of DW depinning P_D is determined as a function of the static magnetic field B_e, the amplitude j_a, and the frequency f_j of applied current by computing 25 stochastic realizations for each set of parameters (B_e, j_a, f_j).

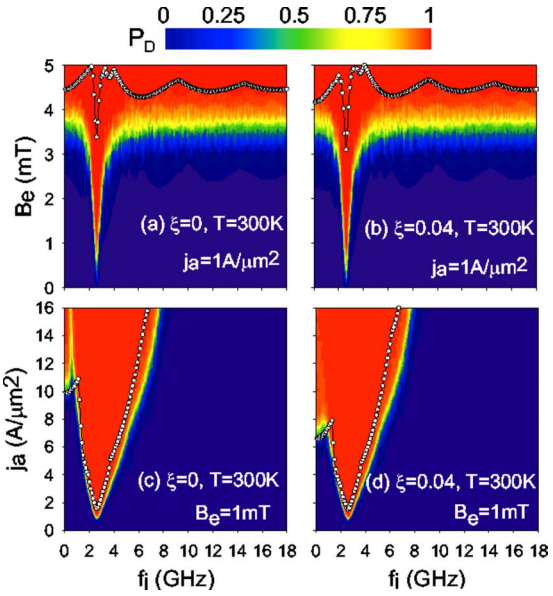

FIG. 8. (Color online) Probability of DW depinning P_D at room temperature $T=300$ K subjected to static fields B_e and ac's of various amplitudes j_a and frequencies f_j. Adiabatic ($\xi=0$) and nonadiabatic ($\xi=0.04$) results are depicted in the left and right columns, respectively. Top panels (a) and (b) show P_D at a constant amplitude of the current of ($j_a=1$ A/μm^2) versus magnetic field B_e and frequency f_j. Bottom panels (c) and (d) show P_D at a constant field ($B_e=1$ mT) versus j_a and frequency f_j. Open symbols correspond to the deterministic depinning curves shown in Fig. 7.

Maps of P_D at room temperature are shown in the top panels of the Fig. 8 for ac's of constant amplitude $j_a=1$ A/μm^2 as a function of the frequency f_j and the static magnetic field B_e. Left panel (a) corresponds to the perfect adiabatic limit ($\xi=0$), and the right one (b) presents the nonadiabatic case with $\xi=0.04$. In the same manner as in the deterministic case, the DW is thermally depinned at $T=300$ K with minimum field at resonance ($f_j=f_N$), for both adiabatic and nonadiabatic cases. In both cases, thermal fluctuations significantly reduce the minimum field, which promotes DW depinning as compared to the deterministic case (see the line with open symbols corresponding to $T=0$) in the whole frequency range. At the resonance frequency, the depinning field is significantly reduced as due to thermal fluctuations, i.e., B_{dep} decreases from 3.4 mT at $T=0$ to 0.75 mT at $T=300$ K in the perfect adiabatic limit, which represents a reduction of the 78%. A reduction of the 80% in the depinning field is observed for $\xi=0.04$ in the resonance as due to thermal fluctuations. This analysis points out the key role of thermal fluctuations on the DW depinning. The stochastic results presented in Figs. 8(a) and 8(b) are in good agreement with recent experiments: see, for example, Figs. 2(E)–2(G) in Ref. 3, where the depinning field was efficiently reduced by means of a train of rectangular current pulses of fixed amplitude with a duration tuned to the characteristic period of the DW oscillations.

The bottom panels of Fig. 8 show the probability of DW depinning P_D at room temperature for a constant field of $B_e=1$ mT as a function of f_j and j_a of the ac's. The left panel [Fig. 8(c)] corresponds to the perfect adiabatic limit ($\xi=0$),

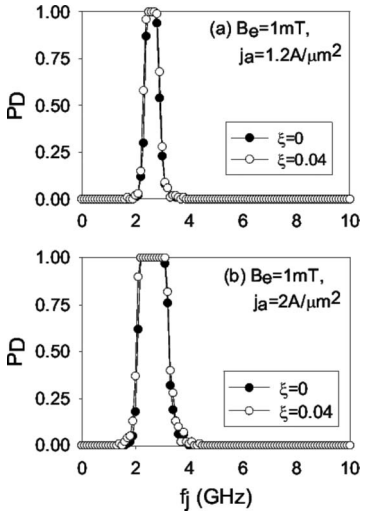

FIG. 9. Probability of DW depinning P_D at room temperature $T=300$ K as a function of f_j under a fixed static field of $B_e=1$ mT for two different amplitudes of the applied current: (a) $j_a=1.2$ A/μm^2 and (b) $j_a=2$ A/μm^2. Adiabatic ($\xi=0$) and nonadiabatic ($\xi=0.04$) results are displayed by filled and open symbols, respectively.

and the right one [Fig. 8(d)] depicts the results for the nonadiabatic case with $\xi=0.04$. As in the deterministic case, the depinning current reaches a minimum value at resonance. For the perfect adiabatic case at resonance ($f_j=f_N$), the critical depinning current decreases from 1.6 A/μm^2 at zero temperature to 1 A/μm^2 at room temperature, which corresponds to a reduction of 37.5%. In the nonadiabatic case, the critical depinning current decreases from 1.5 A/μm^2 at zero temperature to 1 A/μm^2 at room temperature, which corresponds to a reduction of 40%. These percentages are around half than the one observed for the depinning field under constant amplitude of the current, which indicates that thermal fluctuations are less important on reducing the critical depinning current under a fixed field.

The frequency dependence of the depinning probability P_D shown in Fig. 8 is presented in more detail in Fig. 9 for a fixed magnetic field $B_e=1$ mT and two different amplitudes of the current. As can be observed, the transition from the pinned state to the depinned one is highly selective in the frequency domain. In particular, if the amplitude of the current is fixed to $j_a=1.2$ A/μm^2 [Fig. 9(a)], the DW is depinned with 100% of probability for frequencies in the range $2.4 \leqslant f_j \leqslant 2.6$ GHz, and P_D abruptly decreases to 0 if the frequency is reduced (augmented) to 1.9 GHz (3 GHz). If the current is increased to $j_a=2$ A/μm^2 [Fig. 9(b)], the full probability depinning range becomes broader, but more importantly, the pinned-depinned transition continues to occur in a very narrow frequency range. This observation constitutes a relevant prediction for technological applications because it indicates that the DW depinning can be achieved in a very selective manner just by tuning the frequency of the ac.

In order to describe the effect of the temperature on the DW depinning, we have computed the first value of the applied field for which the probability of DW depinning is of

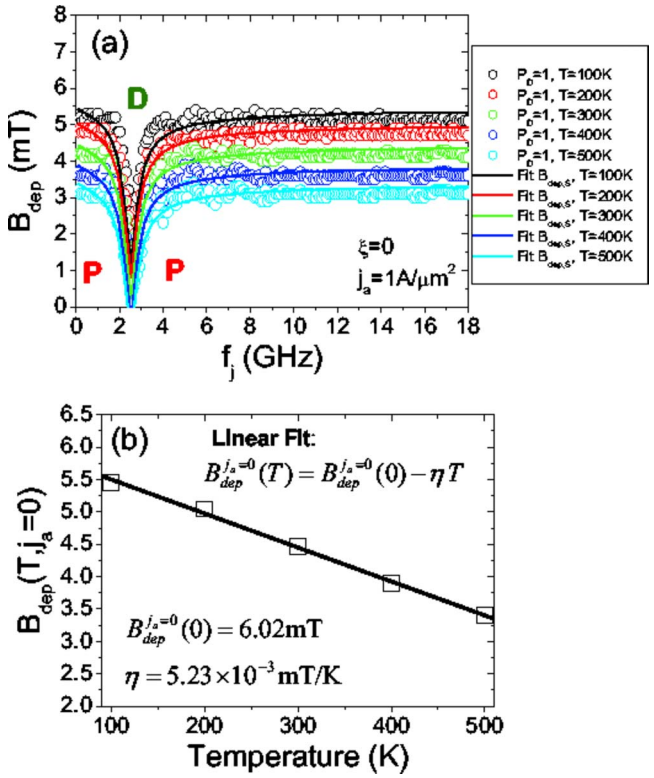

FIG. 10. (Color online) (a) Critical depinning fields at different temperatures. Open symbols correspond to first field B_e at which $P_D=1$, whereas lines represent the fittings to the stationary depinning field given by Eq. (7). The results were computed assuming perfect adiabatic conditions ($\xi=0$), and the amplitude of the ac is fixed to $j_a=1$ A/μm^2. (b) Temperature dependence of the depinning field at zero current ($B_{dep}(T,j_a=0)\equiv B_{dep}^{j_a=0}(T)$) obtained from the fittings to the stationary depinning curves.

100% ($P_D=1$) for each frequency f_j and for different temperatures. The results are depicted by means of dots in Fig. 10 for the perfect adiabatic case ($\xi=0$) when the amplitude of the applied current is fixed to $j_a=1$ A/μm^2. These dots present the same features than the stationary depinning field given by Eq. (7). Therefore, we can deduce the temperature dependence of the depinning field in the absence of current $B_{dep}^{j_a=0}(T)$ by fitting the stochastic results to Eq. (7). The results of these fittings are shown in the inset of Fig. 10, which indicates that $B_{dep}^{j_a=0}(T)$ decreases linearly with the temperature according to $B_{dep}^{j_a=0}(T)=B_{dep}^{j_a=0}(0)-\eta T$, where $B_{dep}^{j_a=0}(0)=6.02$ mT and $\eta=5.26\times10^{-3}$ mT/K. Once derived, how the zero-current depinning field $B_{dep}^{j_a=0}(T)$ varies with T, we can straightforwardly use it to estimate the frequency dependence of the depinning field at any temperature under any j_a and ξ, just replacing $B_{dep}^{j_a=0}$ by $B_{dep}^{j_a=0}(T)$ in Eq. (7). The same procedure is also valid for estimating the critical depinning current by using Eq. (10).

All previous results show that the most favorable situation to produce DW depinning under ac electric density currents and static magnetic fields is achieved at resonance ($f_j=f_N$). In order to quantify the reduction in the amplitude of the ac with respect to the dc case, the probability of DW depinning

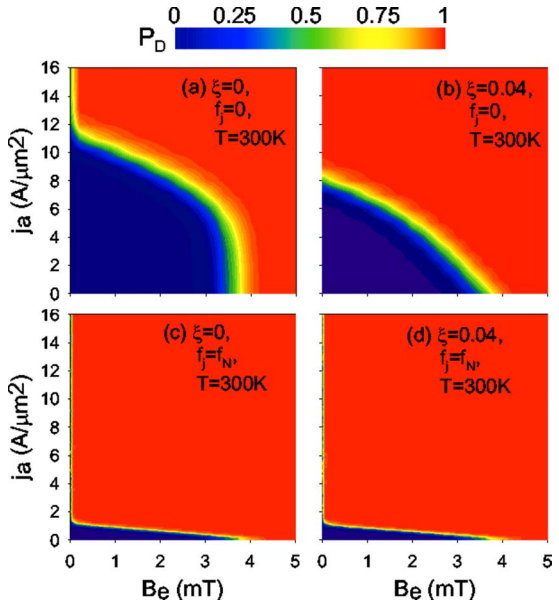

FIG. 11. (Color online) Probability of DW depinning P_D at room temperature $T=300$ K as a function of B_e and j_a. Top panels correspond to dc's, and the bottom ones were computed for the resonance $f_j=f_N$. Adiabatic ($\xi=0$) and nonadiabatic ($\xi=0.04$) results are displayed at $T=300$ K in the left and right panels, respectively.

at room temperature is depicted in Fig. 11 as a function of j_a and B_e. Top panels correspond to the dc case ($f_j=0$), whereas the bottom ones were computed by ac's in the resonance ($f_j=f_N$). In the dc case, P_D is highly sensitive to the nonadiabatic parameter, and the critical current increases monotonously when the field is reduced. For ac's at resonance, the results do not depend very much on the nonadiabatic corrections, and for both adiabatic ($\xi=0$) and nonadiabatic ($\xi=0.04$) cases, the critical depinning current decreases linearly from 1.6 A/μm^2 to 0 when B_e is increased from 0.05 to 3.85 mT. Therefore, the resonant DW depinning can be achieved by means of currents significantly lower than the dc case. This low-current operation has important consequences from a technological point of view because it allows to prevent unwanted effects due to Joule heating.[24] Our results of Fig. 11 can be also compared with recent experimental measures by Thomas *et al.* [see Figs. 3(A)–3(C) in Ref. 30]. Their experiments indicate that even in resonance the DW remains trapped in the notch at the end of the sequence of rectangular pulses in the absence of magnetic field. Although the dimensions of the analyzed strip, and both the shape and size of the notch are quite different from our case, this observation is qualitatively consistent with our results for the perfect adiabatic case [see Fig. 11(c)], where a minimum field of 0.05 mT was required to promote the adiabatic depinning even in the resonance. Apart from this small field range, which depends on the particular shape and depth of the notch, the reduction of the depinning current at resonance predicted by our stochastic 1DM is in good qualitative agreement with the experimental results.

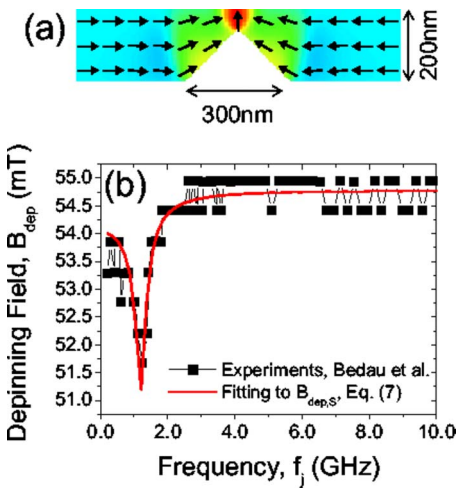

FIG. 12. (Color online) (a) Schematic representation of a transverse DW inside a triangular notch (150 nm high and 300 nm wide) in a Permalloy strip with rectangular cross section (200×25 nm^2). (b) Depinning field as a function of frequency for a constant current density of $j_a=0.02$ A/μm^2. The experimental values by Bedau *et al.* (Ref. 31) are depicted by black squares, and the red line represents the fitting of these experimental values to the stationary depinning field given by Eq. (7) using the following parameters: $M_s=8\times10^5$ A/m, $A=1.3\times10^{-11}$ J/m, $\alpha=0.02$, $P=0.7$, $L_N=400$ nm, $\Delta_0=31$ nm, and $m_w=1.84\times10^{-23}$ kg. The value of the elastic constant $K_N=1.074\times10^{-3}$ N/m was obtained from Eq. (8) by using the experimental values for the depinning field in the absence of current, and the extent of the pinning potential.

IV. COMPARISON WITH THE EXPERIMENTS: EFFECTIVE NONADIABATIC PARAMETER

During the revision process of this manuscript, an experimental work, focused on the resonant DW depinning at low temperature, was published by Bedau *et al.*[31] They experimentally measured the depinning field of a transverse DW as function of the frequency of the injected current considering a triangular notch placed between two electrical contacts in a Permalloy ring ($M_s=8\times10^5$ A/m, $A=1.3\times10^{-11}$ J/m, $\alpha=0.02$, and $P=0.7$). Their observations show similar features to our theoretical results. Therefore, and in order to perform a quantitative comparison with these data, a straight strip with the same cross section (200×25 nm^2) and similar notch geometry (a 300 nm wide and 150 nm deep triangular notch) than in the experiments by Bedau *et al.*[31] has been considered for the micromagnetic simulations [see Fig. 12(a)]. A 31 nm wide transverse wall is deduced when it is positioned in the center of the notch, which corresponds to an effective DW mass of $m_w=1.84\times10^{-23}$ kg. Assuming that the DW width does not change during the depinning process with respect to its value at rest, the experimental values by Bedau *et al.* [see the inset of Fig. 2(a) in Ref. 31] can be straightforward and accurately fitted to Eq. (7). The comparison is displayed in Fig. 12(b), and from this fitting we obtain an effective nonadiabatic parameter of $\xi_{eff}=4.07\pm0.18$. Note that all material parameters are realistic, and ξ_{eff} is the only fitting parameter here.

The effective nonadiabatic parameter ($\xi_{eff}=4.07\pm0.18$) deduced from the fitting of the experimental values is 2 or-

ders of magnitude larger than the predictions done by Zhang and Li[9] and Thiaville *et al.*,[10] where the nonadiabatic parameter was estimated to be around 0.04 from $\xi=\tau_{ex}/\tau_{sf}$, being τ_{ex} the typical *s-d* exchange time ($\tau_{ex}=\hbar/SJ_{ex}$, with J_{ex} representing the exchange interaction energy), and τ_{sf} the characteristic spin-flip time. The origin of this contribution to the nonadiabatic torque is the finite mistracking angle between the conduction electron spin and the local magnetization inside the wall.[9] On the other hand, the theoretical description of Tatara and Kohno[7] puts forward two effects of an electric current across a DW, called spin transfer and momentum transfer, respectively. The spin transfer has the same form than the perfect adiabatic term, and it is expected to be dominant for thick DWs. On the other hand, the momentum transfer enters the integrated DW dynamics similarly to the nonadiabatic term proposed in Refs. 9 and 10, and it was shown to be governed by the DW resistance R_{DW}. For the case of the rigid DW approach, Tatara *et al.*[36] have pointed out that the nonadiabatic product $P\xi$ should be replaced by the effective one $P\xi_{eff}=P\xi+\tilde{R}$, where $\tilde{R}=\Delta_0 e^2 n(L_y L_z)R_{DW}/\hbar$ represents the dimensionless DW resistivity, and $n\approx a^{-3}$ is the electron density, being a the lattice constant. Considering a lattice constant of $a=0.226$ nm ($M_s=gS\mu_B/a^3\approx 8\times 10^5$ A/m, where $S\approx 1/2$, $g\approx 2$), and $\xi=0.04$, we can deduce the DW resistance from the estimated value of the effective nonadiabatic parameter $\xi=4.07$, which yields $R_{DW}=0.86\ m\Omega$. This value is of the same order of magnitude than the one deduced in the experiments of Saitoh *et al.*[27] for the resonant DW oscillations driven by ac's in a different system. The analysis reveals that the momentum transfer dominates over the spin transfer, and it also indicates that the nonadiabaticity is governed by the DW resistance. On the other hand, it would be also interesting to measure the depinning field as a function of the frequency at different temperatures, which could help us to estimate the temperature dependence of both the polarization factor and nonadiabatic parameter. This is far from the scope of this work and it will be treated elsewhere.

V. CONCLUSIONS

In summary, we have firstly presented a micromagnetic characterization of the pinned DW dynamics inside a pinning potential driven by ac's of several amplitude and frequencies, and also assisted by a static field. After a short transient period, the DW reaches a stationary regime describing oscillations with constant amplitude at the same frequency of the driving current. It was found that this amplitude of the DW oscillations increases linearly with the magnitude of the applied current, and it can be resonantly amplified if the driving frequency approaches the characteristic frequency of the pinning potential. Based on these micromagnetic observations, the deterministic DW depinning was analytically evaluated by means of the one-dimensional description, which treats the DW as a rigid particle inside a parabolic potential well. This simple description allows us to understand the resonant amplification of the pinned DW oscillations observed in the previous micromagnetic analysis. The predictions of the 1DM for the DW depinning were studied in several cases both at zero and at room temperature. In general, thermal fluctuations favor the DW depinning with respect to the deterministic case, but more importantly, a noticeable reduction of the required depinning current and field was observed in the resonance with respect to the dc case. This fact could be of relevance for technological applications because it shows that DW depinning is with much more reduced current than in the dc case, avoiding undesirable effects associated with Joule heating. The probability of DW depinning changes abruptly from 0% to 100% in a very narrow range of frequencies at room temperature, which constitutes another relevant result from a technological point of view because it makes the DW depinning highly selective in the frequency range. On the other hand, the formalism here developed can be used to gain understanding of recent experimental results, and in particular, the effective value of the nonadiabatic parameter during the depinning process can be inferred. On the other hand, the temperature dependence of both the polarization factor and the nonadiabaticity could be deduced by using the formalism here developed to fit the experimental results of the depinning process measured at different temperatures.

ACKNOWLEDGMENTS

We thank M. Klaui for providing his experimental data and for useful comments. This work was partially supported by projects MAT2005-04827 from Spanish government and SA063A05 from Junta de Castilla y Leon.

APPENDIX A: ANALYTICAL SOLUTION

Equation (2) is a second-order differential equation describing the damped DW dynamics driven by the external forces (5) and (6) inside of a parabolic potential well. The general solution of Eq. (2) has a transient $x_T(t)$ and a stationary $x_S(t)$ part,

$$x(t)=x_T(t)+x_S(t). \tag{A1}$$

The homogeneous differential equation of motion is the remaining equation (2) in the absence of external driving forces ($F_{e,s}=F_{e,d}=0$), that is, for $B_e=j_{app}(t)=0$. The transient solution $x_T(t)$ is the solution to this homogeneous differential equation, which has to be combined with the particular solution $x_S(t)$ and forced to fit the initial conditions of the problem. The form of this transient solution is that of the free damped oscillator, which can be underdamped [$(b/2m_w)^2<\omega_N^2$], overdamped [$(b/2m_w)^2>\omega_N^2$], or critically damped [$(b/2m_w)^2=\omega_N^2$]. It is easy to verify that for our parameters, the underdamped condition is fulfilled. Therefore, the transient part $x_T(t)$ can be written as

$$x_T(t)=A_T e^{-(b/2m_w)t}\cos(\omega_T t+\phi_T), \tag{A2}$$

where ω_T is given by

$$\omega_T=\sqrt{\omega_N^2-\left(\frac{b}{2m_w}\right)^2} \tag{A3}$$

and A_T and ϕ_T are arbitrary constants, which depend on the initial conditions.

Due to the exponential factor in Eq. (A2), the amplitude of the transient oscillations decays very fast, and for sufficiently larger times, the position reaches a stationary regime consisting of forced oscillations of constant amplitude and varying in time at the same frequency f_j as the ac driving force. The stationary solution $x_S(t)$ is the particular solution of the inhomogeneous differential equation of motion ($B_e \neq 0, j_{app}(t) \neq 0$). It is determined by the driving forces (5) and (6) independently of the initial conditions. Under the action of static fields B_e and oscillating ac's in the form $j_{app}(t)=j_a \cos(2\pi f_j t)$, the particular solution $x_S(t)$ of Eq. (2) is given by

$$x_S(t) = x_{eq,H} + A_S \cos(\omega_j t - \delta_S), \tag{A4}$$

where $\omega_j=2\pi f_j$, and $x_{eq,H}$ represents the equilibrium position reached under static magnetic field, which is given by

$$x_{eq,H} = \frac{F_{H,s}}{K_N} = \frac{(\mu_0 L_y L_z) 2M_s H_e}{K_N}. \tag{A5}$$

A_S is the amplitude of forced oscillations in the stationary regime, and δ_S represents the phase between the applied current $j_{app}(t)$ and the DW position $x(t)$ in the stationary regime. By imposing the particular solution (A4) in the general equation (2), A_S and δ_S can be expressed as

$$A_S = -\frac{1}{m_w}(\mu_0 L_y L_z)\frac{2M_s}{\gamma_0 \Delta_0}\frac{\mu_B P}{e M_s} j_a \sqrt{\frac{\xi^2 + (1+\alpha\xi)^2 \dfrac{\omega_j^2}{\omega_d^2}}{(\omega_N^2 - \omega_j^2)^2 + \left(\dfrac{b}{m_w}\right)^2 \omega_j^2}}, \tag{A6}$$

$$\delta_S = \arctan\left\{ \omega_j \left[\frac{\xi b \omega_d - (1+\alpha\xi) m_w (\omega_N^2 - \omega_j^2)}{m_w \xi \omega_d (\omega_N^2 - \omega_j^2) + (1+\alpha\xi) b \omega_j^2} \right] \right\}, \tag{A7}$$

where $\omega_d=\gamma_0 M_s(N_z-N_y)$ is the angular frequency of the magnetization oscillations around the demagnetizing field inside the wall.

Finally, A_T and ϕ_T are real constants, which have to be determined from the initial conditions. Based on our micromagnetic simulations, the initial DW position and velocity are $x(0)=0$ and $v(0)=-\frac{b_J(0)}{1+\alpha^2}$, respectively. Imposing these initial conditions in the general solution (A1) with Eqs. (A2) and (A4), the constants A_T and ϕ_T can be expressed in terms of the stationary amplitude A_S, the stationary phase δ_S, and the natural frequency of the transient ω_T as follows:

$$\phi_T = \arctan\left\{ \frac{1}{\omega_T} \left[\frac{v(0) - \omega_j A_S \sin(\delta_S)}{(x_{eq,H} + A_S \cos(\delta_S))} - \frac{b}{2m_w} \right] \right\}, \tag{A8}$$

$$A_T = -\frac{1}{\cos(\phi_T)}[x_{eq,H} + A_S \cos(\delta_S)]. \tag{A9}$$

The general solution (A1) with Eqs. (A2) and (A2) describes the temporal evolution of the DW position inside an infinite harmonic potential well from a linearized one-dimensional point of view. Our parabolic potential has a finite extension given by L_N. Except where the contrary is said, the deterministic depinning curves were computed by evaluating the general solution (A1) with Eqs. (A2) and (A4), and the DW depinning takes place at a given time if $x(t) \geqslant L_N$. Once depinned from the notch, the DW freely propagates with an average velocity given solely by the external field ($[v]_T \equiv \frac{1}{T}\int_0^T v(t)dt = \frac{\gamma_0 \Delta_0 H_e}{\alpha}$) because the averaged effect of the oscillating current is zero in a period. In the particular case of dc's ($\omega_j=0$), $\delta_S=0$, the stationary amplitude given by Eq. (A6) reduces to $A_S(f_j=0) \equiv x_{eq,j} \equiv \frac{F_{j,s}}{K_N}$, where $x_{eq,j}$ represents the terminal equilibrium position reached under dc, which evidently is only no null for finite nonadiabatic corrections ($\xi > 0$), in agreement with micromagnetic simulations.

*Corresponding author; emvecino@ubu.es

[1] L. Berger, Phys. Lett. **46A**, 3 (1973).
[2] L. Berger, J. Appl. Phys. **49**, 2156 (1978).
[3] L. Berger, J. Appl. Phys. **55**, 1954 (1984).
[4] J. Slonczewski, J. Magn. Magn. Mater. **159**, L1 (1996).
[5] J. Slonczewski, J. Magn. Magn. Mater. **195**, L261 (1999).
[6] Ya. B. Bazaliy, B. A. Jones, and Shou-Cheng Zhang, Phys. Rev. B **57**, R3213 (1998).
[7] G. Tatara and H. Kohno, Phys. Rev. Lett. **92**, 086601 (2004).
[8] Z. Li and S. Zhang, Phys. Rev. B **70**, 024417 (2004).
[9] S. Zhang and Z. Li, Phys. Rev. Lett. **93**, 127204 (2004).
[10] A. Thiaville, Y. Nakatani, J. Miltat, and S. Suzuki, Europhys. Lett. **69**, 990 (2005).
[11] S. E. Barnes and S. Maekawa, Phys. Rev. Lett. **95**, 107204 (2005).
[12] Z. Li, J. He, and S. Zhang, J. Appl. Phys. **99**, 08Q702 (2006).

[13] E. Martinez, L. Lopez-Diaz, L. Torres, C. Tristan, and O. Alejos, Phys. Rev. B **75**, 174409 (2007).
[14] E. Martinez, L. Lopez-Diaz, O. Alejos, L. Torres, and C. Tristan, Phys. Rev. Lett. **98**, 267202 (2007).
[15] M. Klaui, P. O. Jubert, R. Allenspach, A. Bischof, J. A. C. Bland, G. Faini, U. Rudiger, C. A. F. Vaz, L. Vila, and C. Vouille, Phys. Rev. Lett. **95**, 026601 (2005).
[16] M. Laufenberg, W. Buhrer, D. Bedau, P. E. Melchy, M. Klaui, L. Vila, G. Faini, C. A. F. Vaz, J. A. C. Bland, and U. Rudiger, Phys. Rev. Lett. **97**, 046602 (2006).
[17] M. Hayashi, L. Thomas, Ya. B. Bazaliy, C. Rettner, R. Moriya, X. Jiang, and S. S. P. Parkin, Phys. Rev. Lett. **96**, 197207 (2006).
[18] G. S. D. Beach, C. Knutson, C. Nistor, M. Tsoi, and J. L. Erskine, Phys. Rev. Lett. **97**, 057203 (2006).
[19] G. Meier, M. Bolte, R. Eiselt, B. Kruger, Dong-Hyun Kim, and P. Fischer, Phys. Rev. Lett. **98**, 187202 (2007).
[20] S. S. P. Parkin, U.S. Patent No. 6,834,005 (21 December 2004).
[21] M. Tsoi, R. E. Fontana, and S. S. P. Parkin, Appl. Phys. Lett. **83**, 2617 (2003).
[22] M. Klaui, C. A. F. Vaz, J. A. C. Bland, W. Wernsdorfer, G. Faini, E. Cambril, L. J. Heyderman, F. Nolting, and U. Rudiger, Phys. Rev. Lett. **94**, 106601 (2005).
[23] D. Ravelosona, D. Lacour, J. A. Katine, B. D. Terris, and C. Chappert, Phys. Rev. Lett. **95**, 117203 (2005).
[24] M. Hayashi, L. Thomas, C. Rettner, R. Moriya, X. Jiang, and S. S. P. Parkin, Phys. Rev. Lett. **97**, 207205 (2006).
[25] L. Thomas, M. Hayashi, X. Jiang, R. Moriya, C. Rettner, and S. S. P. Parkin, Nature (London) **443**, 197 (2006).
[26] P. Dagras, M. Klaui, M. Laufenberg, D. Bedau, L. Vila, G. Faini, C. A. F. Vaz, J. A. C. Bland, and U. Rudinger, J. Phys. D **40**, 1247 (2007).
[27] E. Saitoh, H. Miyajima, T. Yamaoka, and G. Tatara, Nature (London) **432**, 203 (2004).
[28] G. Tatara, E. Saitoh, M. Ichimura, and H. Kohno, Appl. Phys. Lett. **86**, 232504 (2005).
[29] Peng-Bin He, X. C. Xie, and W. M. Liu, Phys. Rev. B **72**, 172411 (2005).
[30] L. Thomas, M. Hayashi, X. Jiang, R. Moriya, C. Rettner, and S. S. P. Parkin, Science **315**, 1553 (2007).
[31] D. Bedau, M. Klaui, S. Krzyk, U. Rudiger, G. Faini, and L. Vila, Phys. Rev. Lett. **99**, 146601 (2007).
[32] N. L. Schryer and L. R. Walker, J. Appl. Phys. **45**, 5406 (1974).
[33] The DW width is computed according to Porter's definition $\pi\Delta_0 = L_x\sqrt{\langle m_y\rangle^2 + \langle m_z\rangle^2}$ [see Eqs. (11)–(13) in D. G. Porter and M. J. Donahue, J. Appl. Phys. **95**, 6729 (2004)]. A value of $\Delta_0 = 21.14$ nm was obtained in the absence of field and current.
[34] R. A. Duine, A. S. Nunez, and A. H. MacDonald, Phys. Rev. Lett. **98**, 056605 (2007).
[35] A. Aharoni, J. Appl. Phys. **83**, 3432 (1998).
[36] G. Tatara, T. Takayama, H. Kohno, J. Shibata, Y. Nakatani, and H. Fukuyama, J. Phys. Soc. Jpn. **75**, 064708 (2006).